ELSEVIER

Earth and Planetary Science Letters 188 (2001) 459–474

EPSL

www.elsevier.com/locate/epsl

Erosion of Deccan Traps determined by river geochemistry: impact on the global climate and the $^{87}Sr/^{86}Sr$ ratio of seawater

Céline Dessert [a,*], Bernard Dupré [a], Louis M. François [a,b], Jacques Schott [a], Jérôme Gaillardet [c], Govind Chakrapani [a,d], Sujit Bajpai [e]

[a] *LMTG, Université Paul Sabatier, 38 rue des 36 Ponts, 31400 Toulouse, France*
[b] *LPAP, Université de Liège, 5 avenue de Cointe, 4000 Liège, Belgium*
[c] *Laboratoire de Géochimie et Cosmochimie, IPGP, 4 place Jussieu, 75005 Paris, France*
[d] *Department of Earth Sciences, University of Roorkee, Roorkee 247667, India*
[e] *School of Environmental Sciences, Jawaharlal Nehru University, New Delhi 110 067, India*

Received 21 November 2000; accepted 19 March 2001

Abstract

The impact of the Deccan Traps on chemical weathering and atmospheric CO_2 consumption on Earth is evaluated based on the study of major elements, strontium and $^{87}Sr/^{86}Sr$ isotopic ratios of the main rivers flowing through the traps, using a numerical model which describes the coupled evolution of the chemical cycles of carbon, alkalinity and strontium and allows one to compute the variations in atmospheric pCO_2, mean global temperature and the $^{87}Sr/^{86}Sr$ isotopic ratio of seawater, in response to Deccan trap emplacement. The results suggest that the rate of chemical weathering of Deccan Traps (21–63 t/km^2/yr) and associated atmospheric CO_2 consumption ($0.58–2.54\times10^6$ mol C/km^2/yr) are relatively high compared to those linked to other basaltic regions. Our results on the Deccan and available data from other basaltic regions show that runoff and temperature are the two main parameters which control the rate of CO_2 consumption during weathering of basalts, according to the relationship:

$$f = R_f \times C_0 \exp\left[\frac{-Ea}{R}\left(\frac{1}{T}-\frac{1}{298}\right)\right]$$

where f is the specific CO_2 consumption rate (mol/km^2/yr), R_f is runoff (mm/yr), C_0 is a constant (= 1764 μmol/l), Ea represents an apparent activation energy for basalt weathering (with a value of 42.3 kJ/mol determined in the present study), R is the gas constant and T is the absolute temperature (°K). Modelling results show that emplacement and weathering of Deccan Traps basalts played an important role in the geochemical cycles of carbon and strontium. In particular, the traps led to a change in weathering rate of both carbonates and silicates, in carbonate deposition on seafloor, in Sr isotopic composition of the riverine flux and hence a change in marine Sr isotopic composition. As a result, Deccan Traps emplacement was responsible for a strong increase of atmospheric pCO_2 by 1050 ppmv followed by a new steady-state pCO_2 lower than that in pre-Deccan times by 57 ppmv, implying that pre-industrial atmospheric pCO_2 would have been 20% higher in the absence of Deccan basalts. pCO_2 evolution was accompanied by a rapid

* Corresponding author. Fax: +33-5-61-55-81-38; E-mail: dessert@lmtg.ups-tlse.fr

0012-821X/01/$ – see front matter
PII: S0012-821X(01)00317-X

warming of 4°C, followed after 1 Myr by a global cooling of 0.55°C. During the warming phase, continental silicate weathering is increased globally. Since weathering of continental silicate rocks provides radiogenic Sr to the ocean, the model predicts a peak in the $^{87}Sr/^{86}Sr$ ratio of seawater following the Deccan Traps emplacement. The amplitude and duration of this spike in the Sr isotopic signal are comparable to those observed at the Cretaceous–Tertiary boundary. The results of this study demonstrate the important control exerted by the emplacement and weathering of large basaltic provinces on the geochemical and climatic changes on Earth.

Keywords: erosion; rivers; geochemistry; Sr-87/Sr-86; Deccan Traps; Global change; weathering; paleoclimatology; K-T boundary

1. Introduction

Continental erosion is a major geological process which is responsible for landscape evolution and exerts a major control on the transport of erosion matters from continents to the oceans and on the cycles of many chemical elements, including carbon, at the Earth's surface. Moreover, as chemical weathering involves consumption of atmospheric CO_2, a greenhouse gas, it probably strongly influences the secular evolution of the Earth's climate.

Over geologic time scales, three major processes consume atmospheric CO_2: (1) the chemical weathering of continental silicate rocks [1–3], (2) the organic carbon burial during sediment deposition (e.g. [4–6]) and (3) the chemical weathering of the oceanic crust [7,8].

Because climatic conditions are dependent on the atmospheric CO_2 levels, several authors have tried to model the evolution of the carbon cycle and other elements over geologic time [2,8–10]. In order to quantify the role of silicate weathering in the carbon cycle, it is necessary to study the geochemistry of rivers and to determine the laws governing chemical weathering. Many studies have focused on river geochemistry on a global [1,11–18] and smaller scale [19–23]. These studies suggest lithology to be a dominant parameter which controls intensity of erosion and atmospheric CO_2 consumption, followed by climatic parameters (runoff and temperature). The importance of lithology is emphasised in the studies of Meybeck [19] and Amiotte-Suchet and Probst [24] wherein it is pointed out that granite and gneiss are less easily erodible and hence consume less CO_2 compared to the volcanic rocks. In recent years, weathering of basaltic rocks has been addressed in several studies, in particular those of Louvat [21,25] on four volcanic islands: Iceland, Java, la Réunion and Sao Miguel, and that of Gislason et al. [20] on Iceland. These authors have shown that basaltic weathering is a major CO_2 sink on time scales of several million years because basaltic rocks weather easily. Furthermore, Taylor and Lasaga [26] have shown, from the modelling of the Columbia River basalt, that weathering of large igneous provinces can play a significant role in the evolution of the marine Sr isotope record.

The aim of this study was to quantify the influence of the weathering of the Deccan Traps on the chemistry of seawater and the atmospheric CO_2 mass balance. With this purpose, we studied river geochemistry in the Deccan Traps, one of the largest continental flood basalts on Earth, erupted around 65.5 Myr ago close to the time of the Cretaceous–Tertiary boundary (KT boundary [27,28]). The present-day rates of erosion and atmospheric CO_2 consumption are approximated from the chemistry and the Sr isotope composition of the main rivers draining the Deccan Traps. These results are used in a model presented in this study to calculate the evolution of atmospheric CO_2, global surface temperature, carbonate deposition on seafloor and Sr isotopic composition of seawater following Deccan Traps emplacement. To validate the model, the simulation of oceanic $^{87}Sr/^{86}Sr$ evolution is compared with the actual marine Sr isotope record around the KT boundary [29–31].

2. General setting of Deccan Traps

The Deccan volcanic province is located in the

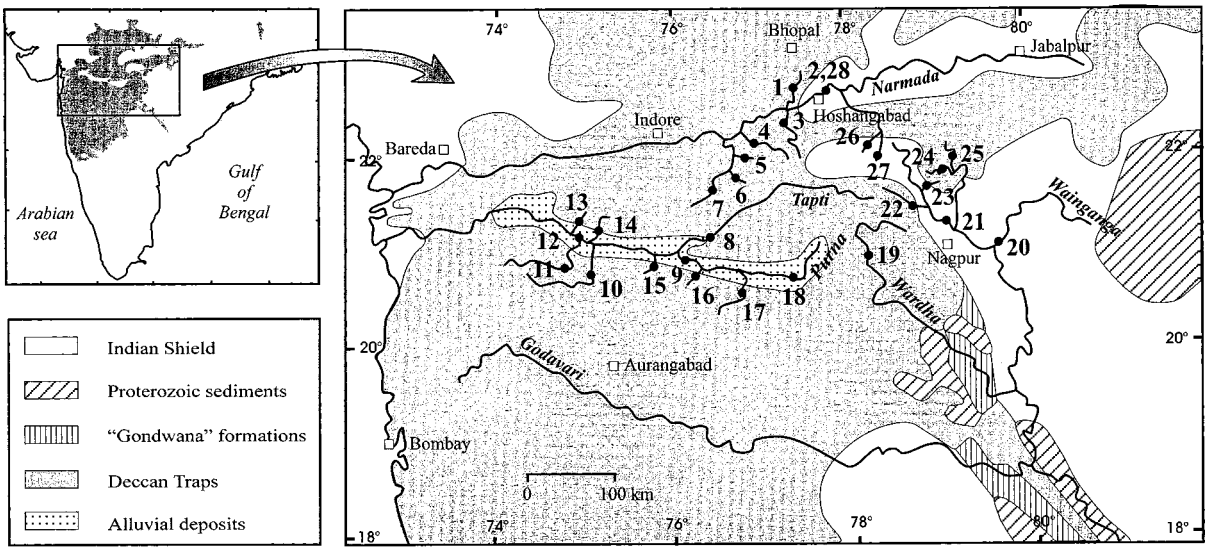

Fig. 1. Location of sampling points in the Deccan Traps volcanic province.

western and central parts of India (Fig. 1). These traps form a high plateau with an average elevation of 750 m. Presently, western India is exposed to a monsoonal climate. The most humid period, between June and September, witnesses the major part of the annual rainfall, with a maximum in July (1150 mm). The temperature is relatively high with an annual mean of 25°C and a maximum in May (35°C).

K–Ar, ^{40}Ar–^{39}Ar and recent Re–Os geochronology coupled with palaeomagnetic and palaeontological studies suggest that the Deccan Traps were erupted around the KT boundary 65.5 Myr ago [27,28,32], when the Indian plate was moving northwards [33]. This volcanic event was apparently quite short on a geological time scale, spanning less than 1 Myr.

The Deccan Traps are one of the largest basaltic provinces on the Earth's surface. They have a present-day volume of $\sim 10^6$ km^3 and cover an area of $\sim 5\times 10^5$ km^2. Courtillot et al. [27] suggested that the total initial volume of lava may have reached $\sim 3\times 10^6$ km^3. Therefore, some two thirds of the initial basalt must have disappeared in the last 65 Myr. The thickness of the lava pile varies from 200 m or less in the east to 1500–2000 m in the west [27,34]. Javoy and Michard [35] estimated that the total amount of CO_2 outgassed during eruption was 1.6×10^{18} mol, which would represent half of the total ocean content.

The western Deccan Traps have been extensively studied in terms of geochemistry and stratigraphy [34,36–38]. Basalts overlie crystalline basement consisting largely of granites and gneisses, and sediments. The basalts are mainly of tholeiitic composition and contain phenocrysts of plagioclase, clinopyroxene, altered olivine, opaque minerals and altered glass. Stratigraphy is based on the chemical and/or isotopic composition of the flows. The basaltic sequence is divided into five sub-horizontal distinct formations: from base to top, the Bushe, Poladpur, Ambenali, Mahabaleshwar and Panhala. The lowermost formations have high Sr isotopic ratios, with all Bushe formations having $^{87}Sr/^{86}Sr$ values higher than 0.713 and all Poladpur formations having $^{87}Sr/^{86}Sr$ values in the range 0.705–0.713. The other three formations have $^{87}Sr/^{86}Sr$ values around 0.705 [34,36]. Older sequences outcrop in the north, with a progressive overstepping, and younger towards the south [34,38]. Cox and Hawkesworth [36] have shown that observed chemical variations are due to heterogeneity of mantle sources, variations in the degree of crustal contamination and effects of fractional crystallisation. These formations are separated in some instances

by lateritic soil horizon and regional lateritic carapaces are preserved in the coastal region [39].

3. Field and laboratory techniques

3.1. Sampling

Water and suspended and bottom sediments were collected during July 1998 in three significant watersheds, namely the Godavari, Narmada and Tapti (Fig. 1). The Godavari drainage area is dominated by basaltic rocks associated with crystalline rocks of the Indian Shield, 'Gondwana' sediments and Proterozoic sediments. The main tributaries are the Wardha (referring to no. 19 in Fig. 1) and the Pench (no. 25). The Wainganga (no. 20) and the Kanhan (no. 21) do not flow through any basaltic lithology and the Ramakona (no. 23) partly drains basalts. The Narmada was sampled twice within an interval of 10 days (no. 2 and no. 28). All Narmada sampled tributaries drain basaltic rocks except the Silverfall (no. 26) and the Denwa (no. 27). The Tapti (no. 8 and no. 12) drains only Deccan Traps and the Purna (no. 9 and no. 18) is its main tributary.

3.2. Analyses

pH and alkalinity were measured in the field during sampling. The alkalinity was determined by acid–base titration (Gran method). Water samples were filtered on site through 0.2 μm cellulose acetate filters (142 mm diameter) using a Sartorius filtration unit made of Teflon. Filtered samples were acidified to pH 2 with HNO_3 and stored in acid-washed polypropylene bottles. The samples for anion determination were not acidified.

Anions and cations were measured by ion chromatography with a precision better than 5%. The accuracy of the analysis was assessed by running the SLRS-3 and the SLRS-4 riverine standards. Dissolved silica concentrations were determined by spectrophotometric measurement. Trace elements were measured by ICP-MS after addition of an indium standard solution. $^{87}Sr/^{86}Sr$ isotopic ratios were determined using mass spectrometry.

4. Results

Concentrations of major elements and Sr isotopic compositions are listed in Table 1. The river waters are mostly alkaline with pH ranging from 7.54 to 8.15. Waters sampled in rivers flowing through the basaltic terrains have high ionic charge ($\Sigma^+ \sim 1839$–6312 μeq/l) and those draining partly through sediments and crystalline rocks have lower ionic charge (153–2722 μeq/l). Waters are characterised by their specific charge balance, as indicated by the normalised inorganic charge balance ($NICB = (\Sigma^+ - \Sigma^-)/\Sigma^+$). Values are generally close to 5%, except for the Ramakona (no. 23) and Kulbakera (no. 24), where the imbalance can be attributed to less precise alkalinity measurements in the field. In these cases, we recalculated the alkalinity from the charge balance.

The dissolved silica concentration varies between 187 and 836 μmol/l for the rivers draining basalts, and between 100 and 314 for other rivers. Concentrations in rivers flowing through the Deccan Traps are similar to those for Réunion Island rivers (200–800 μmol/l [21]). HCO_3^- (1148–5494 μmol/l) is always the dominant anion species, followed by Cl^- (53–1568 μmol/l), SO_4^{2-} (10–268 μmol/l), NO_3^- (4–141 μmol/l), and F^- (1.8–21 μmol/l). The lower anionic concentration characterises rivers draining sediments and crystalline rocks. This observation is also true for cationic content. Among major cations, Na^+ is dominant (47–2794 μmol/l). Ca^{2+} (31–919 μmol/l) and Mg^{2+} (17–1271 μmol/l) have the same range of concentrations whereas concentrations of K^+ range between 7 and 163 μmol/l. The sum of Na^+ and K^+ represents around 28% of the total cation charge. The cation concentrations are lower than those reported in a previous study on the Narmada and Tapti rivers (e.g. $Na^+ \sim 450$–7600 μmol/l [40]). This difference can be explained by the fact that sampling for the previous study was performed in May, when river discharge is lower compared to that during the south west monsoon period.

The concentrations of Sr vary between 1.13 and 3.51 μmol/l for rivers draining basaltic lithology and between 0.07 and 1.47 for the other rivers.

Table 1
Chemical composition of dissolved load

Sample and location	pH	Na	NH_4	K	Mg	Ca	F	Cl	NO_3	SO_4	HCO_3	SiO_2	Σ^+	Σ^-	NICB	Sr	$^{87}Sr/^{86}Sr$	Na*	K*	Mg*	Ca*	SO_4*
		μmol/l	μmol/l	μmol/l	μmol/l	μmol/l	μmol/l	μmol/l	μmol/l	μmol/l	μmol/l	μmol/l	μeq/l	μeq/l	%	μmol/l		μmol/l	μmol/l	μmol/l	μmol/l	μmol/l
Kolar (1)	8.3	711	nd	62	472	724	4.4	155	18	40	2912	366	3166	3169	−0.1	1.51		578	60	457	721	32
Narmada (2)	8.1	369	nd	37	365	669	4.2	93	77	26	2338	314	2474	2565	−3.7	1.30	0.711349 ± 8	290	35	356	668	21
Ganjal (3)	7.9	768	nd	50	440	859	3.1	135	8	44	3249	395	3414	3483	−2.0	1.68	0.709770 ± 21	652	47	426	856	37
Machak (4)	8.7	2077	nd	52	1271	588	18.2	372	nd	98	5494	552	5846	6079	−4.0	2.12	0.709435 ± 18	1758	45	1235	581	79
Kalimachak (5)	8.8	1092	nd	98	983	702	9.2	1164	67	138	3039	836	4560	4556	0.1	3.11		95	77	870	681	79
Khagni (6)	8.1	293	1.3	55	377	749	4.0	117	5	28	2394	332	2601	2576	1.0	1.21		193	53	366	746	22
Chotatawa (7)	8.7	906	nd	99	704	638	6.9	413	nd	67	3182	465	3689	3737	−1.3	2.13	0.708198 ± 22	552	92	664	630	46
Tapti (8)	7.9	659	2	62	475	740	3.6	256	54	63	2847	394	3152	3286	−4.3	1.27	0.708200 ± 21	439	58	450	735	50
Purna (9)	8	1323	12.6	113	316	515	6.9	654	28	127	2167	247	3110	3109	0.0	2.01		762	101	253	503	93
Bori (10)	8.3	1271	nd	114	577	827	8.8	514	13	109	3546	414	4192	4301	−2.6	2.34	0.709565 ± 22	830	104	527	818	83
Panjkra (11)	7.8	2794	84	126	735	919	7.7	1569	114	268	4203	445	6312	6452	−2.2	3.51	0.709710 ± 19	1449	97	583	890	188
Tapti (12)	8.1	1517	nd	93	483	649	5.8	623	45	104	3055	360	3873	3940	−1.7	2.20		984	82	422	638	72
Aranawati (13)	8.1	871	nd	50	401	710	4.7	263	28	52	2773	396	3143	3173	−1.0	1.13		646	45	375	706	39
Aner (14)	8.3	873	1.6	38	703	815	4.6	270	28	40	3686	569	3949	4068	−3.0	1.50	0.707584 ± 22	642	33	677	810	26
Wagurr (15)	7.8	382	5.0	113	229	484	3.4	173	nd	42	1555	242	1926	1815	5.8	1.20		234	110	212	481	33
Nalganga (16)	7.9	1139	37.6	163	190	457	4.9	457	132	88	1858	187	2634	2644	−0.4	1.40		747	155	146	449	64
Mun (17)	7.8	743	10.0	98	249	476	3.5	351	141	77	1525	201	2301	2175	5.5	1.60	0.708846 ± 18	442	92	215	470	59
Purna (18)	7.9	785	10.3	83	165	315	5.0	300	18	73	1256	165	1839	1727	6.1	1.20	0.709114 ± 23	528	78	136	309	58
Wardha (19)	8.2	512	nd	71	534	781	5.8	186	4	38	2971	441	3214	3242	−0.9	1.80	0.708387 ± 17	353	67	517	778	28
Wainganga (20)	7.6	172	0.9	43	160	364	3.0	64	nd	19	1148	171	1264	1254	0.8	0.60		117	42	154	363	16
Kanhan (21)	7.9	550	nd	74	309	701	11.9	199	23	87	2149	261	2644	2557	3.3	1.40		380	70	289	698	77
Jam (22)	8.2	383	nd	44	390	852	15.8	130	15	258	2197	348	2910	2874	1.2	1.50	0.711422 ± 23	272	42	377	849	251
Ramakona (23)	7.9	580	nd	64	322	695	13.3	167	34	140	1562	269	2678	2056	23.2	1.50		437	61	306	692	131
Kulbakera (24)	8.1	532	nd	49	351	874	21.0	166	36	53	2151	279	3031	2481	18.1	1.70	0.714930 ± 19	390	46	335	871	45
Pench (25)	8	383	nd	44	389	849	14.2	130	27	268	2057	348	2904	2765	4.8	1.40	0.711439 ± 17	272	41	377	847	261
Silverfall (26)	nm	47	1.5	7	17	31	nd	53	11	10	nm	100	153	83		0.10		2	6	12	30	7
Denwa (27)	nm	88	1.1	31	56	138	1.8	65	26	24	nm	112	508	141		0.30		31	29	49	137	20
Narmada (28)	7.5	204	0.9	38	197	474	3.0	67	nd	21	1547	217	1587	1659	−4.6	0.80	0.710973 ± 19	146	37	191	473	17

* Indicates concentration corrected from the rain input; nd indicates concentration below detection limit; nm indicates concentrations not measured.

The rivers of the Deccan Traps have higher Sr concentrations than those of the basaltic Réunion, Sao Miguel and Iceland islands (0.026–0.5 μmol/l, 0.18–0.79 μmol/l and 0.015–0.85 μmol/l respectively [25]). However, the Sr concentrations measured in this study are similar to those reported for Java island rivers (0.63–4.08 μmol/l [25]). The $^{87}Sr/^{86}Sr$ isotopic ratios of the rivers draining Deccan Traps vary between 0.70758 and 0.71493.

5. Chemical weathering rates and isotopic chemistry of Sr

5.1. Chemical weathering rates

To quantify the chemical weathering rates, the chemical compositions of river are corrected for atmospheric inputs. This correction was carried out using Cl concentrations and oceanic (X)/(Cl) ratio (where X = Na, Mg, SO_4, Ca or K) and assuming that all the Cl content of the dissolved load has an atmospheric origin. This hypothesis is validated by the very low Cl concentrations of basaltic rocks [34,36]. Cl concentrations in the Kalimachak and Panjkra rivers are very high (>1100 μmol/l, Table 1), suggesting an anthropogenic origin for chloride. Therefore, these rivers were not considered in this study. The corrected concentrations of Na, Mg, SO_4, Ca and K are listed in Table 1.

The total dissolved solids (TDS_w) have been calculated from the concentrations of the major dissolved elements (Na, K, Ca, Mg, SiO_2 and SO_4) originating from the weathering of Deccan basalts. TDS_w values range from 46 to 136 mg/l, with a mean value of 81 mg/l (Table 2). From the data of Dekov et al. [41], we have estimated a mean annual runoff value (net flow of water out of watershed) of 463 mm/yr for the Deccan Traps region. This value is similar to that for Narmada (452 mm/yr [40]). From mean runoff and TDS_w values, we have calculated the specific chemical weathering rates (rate per unit surface area) listed in Table 2. These rates range between 21 and 63 t/km^2/yr, with a mean value of 37 t/km^2/yr. The annual average of chemical erosion flux that

Table 2
TDS_w values (total dissolved solid after rain input corrections), chemical erosion rates and associated atmospheric CO_2 consumption rates deduced from the dissolved load for the monolithologic rivers draining Deccan basalts

Sample and location	TDS_w mg/l	Chemical weathering rate t/km^2/yr	CO_2 consumption rate 10^6 mol/km^2/yr
Kolar (1)	80	37	1.35
Ganjal (3)	89	41	1.50
Machak (4)	136	63	2.54
Khagni (6)	67	31	1.11
Chotatawa (7)	90	42	1.47
Tapti (8)	81	37	1.32
Purna (9)	65	30	1.00
Bori (10)	96	44	1.64
Tapti (12)	85	40	1.41
Aranawati (13)	81	38	1.28
Aner (14)	101	47	1.71
Wagurr (15)	52	24	0.77
Nalganga (16)	58	27	0.86
Mun (17)	55	26	0.76
Purna (18)	46	21	0.63
Wardha (19)	83	39	1.38
Jam (22)	96	44	1.02
Kulbakera (24)	75	35	1.25
Pench (25)	97	45	0.95
Mean	81	37	1.26

results from the weathering of the Deccan area is close to 18.5×10^6 t/yr (by considering an area of 5×10^5 km^2 for these basalts). The specific chemical erosion rates for Deccan Traps are higher than those for most of the world's largest rivers (25 t/km^2/yr for the Amazon and 6 t/km^2/yr for the Zaire [3]) or similar to those for several mountainous rivers (42 and 46 t/km^2/yr respectively for the Ganges and the Brahmaputra [3]). If Deccan rivers are compared with other small rivers draining basalts, it appears that chemical weathering rates for Deccan are similar to those for Sao Miguel (35 t/km^2/yr [25]) and Iceland rivers (41 and 55 t/km^2/yr [20,25]). Rivers of Réunion and Java islands exhibit higher chemical weathering rates (102 and 326 t/km^2/yr [21,25]) because of their higher runoff, temperature and relief.

Thus, based on the present study and on studies of other basaltic rivers, we conclude that the weathering of the Deccan Traps and, more generally, of basalts is of great importance to the total flux of chemical elements washed to the ocean.

5.2. *Flux of strontium and $^{87}Sr/^{86}Sr$ isotopic ratios*

The specific flux of strontium derived from the weathering of Deccan Traps ranges between 361 and 1080 mol/km^2/yr, with an average of 751 mol/km^2/yr. The total flux of strontium is equal to 3.75×10^8 mol/yr and corresponds to 3.7% of strontium derived from silicate weathering [3]. It is interesting to note that the Deccan area represents only 0.5% of the total surface of continents. Thus, the flux of strontium originated from the weathering of the Deccan basalts should not be neglected in the global balance of strontium to the ocean.

The $^{87}Sr/^{86}Sr$ isotopic ratios measured in Deccan rivers vary between 0.70758 and 0.71493. $^{87}Sr/^{86}Sr$ in the Kanhan (samples 21–25) is significantly higher (>0.710) than that in the samples from the Tapti and the Narmada basins, where it varies slightly with many tributaries having $^{87}Sr/^{86}Sr$ close to 0.709. All these values reflect the chemical erosion of the basaltic rocks which have unusually high $^{87}Sr/^{86}Sr$ isotopic ratios ranging between 0.705 and 0.715 [34,36]. Therefore, the $^{87}Sr/^{86}Sr$ ratio of rivers draining Deccan Traps is substantially higher than those of volcanic islands studied by Louvat (0.7035–0.7053 [25]).

6. Atmospheric CO_2 consumption by chemical weathering

The consumption rate of atmospheric CO_2 associated with the chemical weathering of basalts was calculated from riverine HCO_3^- concentrations. During the weathering of silicate rocks, all dissolved bicarbonates originate from atmospheric/soil CO_2. Values of CO_2 consumption rates listed in Table 2 are very high, ranging from 0.58 to 2.54×10^6 mol/km^2/yr with a mean value of 1.26×10^6 mol/km^2/yr. The annual average CO_2 consumption that results from the weathering of the Deccan Traps basalt province is close to 0.63×10^{12} mol/yr. The amount of CO_2 consumed by the weathering of Deccan basalts represents 5% of total CO_2 consumption flux derived from silicate weathering [3]. It must be highlighted that this flux is higher than the silicate alkalinity flux determined for the Amazon (2.75% [3]), the Ganges–Brahmaputra system (2.3% [17]) and the Congo (1.7% [3]).

We have plotted in Fig. 2 atmospheric CO_2 consumption rates as a function of runoff for the Deccan region and small rivers draining only basaltic or granitic lithology [19–21,23,25,42]. It can be seen that lithology, runoff and temperature exert a major control on atmospheric CO_2 consumption. It first appears that rivers draining basaltic rocks have higher HCO_3^- concentrations than those draining granitic rocks; HCO_3^- concentrations of 'basaltic rivers' vary between 400 and 2700 μmol/l, whereas those of 'granitic rivers' vary between 40 and 500 μmol/l. Note also that, for a given runoff value, CO_2 consumption rates during basalt weathering are significantly higher than those for granites. This first observation confirms the important influence of the basaltic lithology on CO_2 consumption rates as noted previously by several authors [19–21,24].

Fig. 2 also highlights the influence of runoff and temperature on CO_2 consumption rates by basalts. For a given temperature, bicarbonate

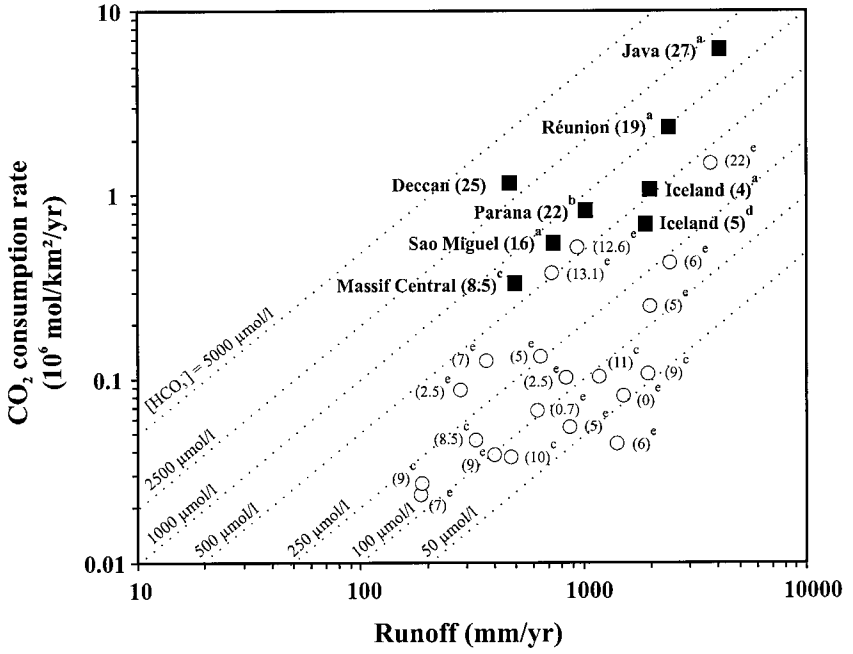

Fig. 2. Plots of mean atmospheric CO_2 consumption rates versus runoff for rivers draining basaltic or granitic lithologies. a: [25]; b: [42]; c: [19]; d: [20]; e: [23]. The values in parentheses correspond to the main surface temperature of each region. Dashed straight lines reported in this figure represent constant HCO_3^- concentrations from 50 to 5000 µmol/l.

concentrations are constant and independent of runoff. Thus, CO_2 consumption rates appear to be approximately proportional to runoff. Unlike runoff, HCO_3^- concentrations are directly dependent on temperature. Indeed, if we consider a constant value of runoff, the observed increase of CO_2 consumption rate reflects an increase of temperature. The temperature effect can be more easily observed in Fig. 3 where, by analogy with experimental studies on the kinetics of mineral weathering, the logarithm of HCO_3^- concentrations has been plotted versus the reciprocal of absolute temperature ($1/T$ in °K) for rivers draining basaltic rocks. A good linear relationship is observed between the two parameters. From the slope of this relation, a value of $Ea = 42.3$ kJ/mol can be deduced for the apparent activation energy of basalt weathering. The relationship between HCO_3^- concentrations and temperature (T) can be defined as:

$$\log C_{HCO_3^-} = -\frac{Ea \times \ln 10}{RT} + b \quad (1)$$

where R represents the gas constant and b the intercept of the linear regression ($= 10.66$). The specific rate of CO_2 consumption of basalts f (mol/km^2/yr) can be expressed as:

$$f = R_f \times C_{HCO_3^-} \quad (2)$$

where R_f (mm/yr) represents the value of runoff. Combining Eqs. 1 and 2 gives:

$$f = R_f \times C_0 \exp\left[\frac{-Ea}{R}\left(\frac{1}{T} - \frac{1}{298}\right)\right] \quad (3)$$

where $C_0 = 10^{(b - Ea/298R\ln 10)} = 1764$ µmol/l.

This equation is not felt to be valid for the weathering rate on granites. In fact, parameters other than runoff and temperature influence the chemical weathering of granites such as soil thickness and physical erosion intensity [13,15,22]; hence, it is difficult to characterise weathering of granite with a simple relation as obtained for basalt.

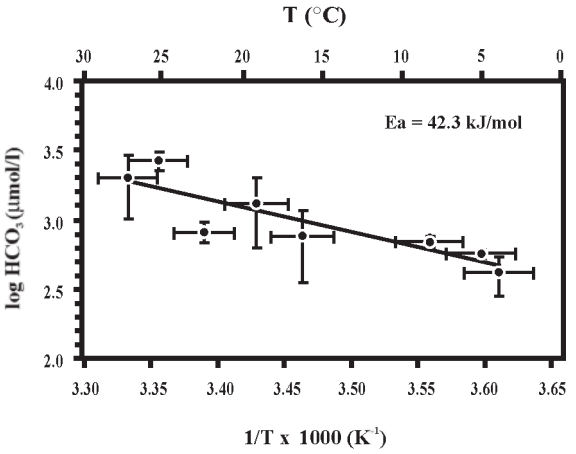

Fig. 3. Logarithm of HCO_3^- concentrations (in µmol/l) versus reciprocal of absolute temperature for rivers draining basaltic rocks [19,20,23,25,42]. From the slope of the linear regression, we estimate an activation energy of 42.3 kJ/mol.

7. Effect of Deccan Traps emplacement on climate and chemistry of oceans

A simple model is next generated to calculate the evolution of atmospheric CO_2 level, surface temperature and strontium isotopic composition of seawater following Deccan Traps emplacement. Using the results inferred from the dissolved load (Section 5) of Deccan Traps rivers, this modelling work allows us to quantify the impact of trap emplacement on global evolution.

7.1. Model description

The model used in this work is a modified and adapted version of those developed by François and Walker [8] and François et al. [43]. In this work, we model the geochemical cycles of inorganic carbon, alkalinity and strontium.

In the case of carbon, the weathering of carbonates (F_{cw}) is the largest source of inorganic carbon. However, this flux is not the primary source driving the evolution of the system, since departures from equilibrium in the weathering–deposition cycle of carbonates remain limited even in the transient experiments performed here. The second source of inorganic carbon is volcanic CO_2 emission. Let F^D_{vol} be the CO_2 emission from Deccan Traps and F^R_{vol} the CO_2 emission from the rest of the world, including mid-ocean ridges. In the model reference simulation, we assume that the time span of Deccan Traps emplacement is 10^5 years [32]. The major sink of inorganic carbon is carbonate deposition on the ocean floor (F_{cd}). This flux is calculated in the model, based on the lysocline depth for calcite and aragonite, in a simple ocean sub-model which is outlined below. In the long term, the carbon budget in a given reservoir is described by a differential equation of the form:

$$\frac{dC_T}{dt} = F^D_{vol} + F^R_{vol} + F_{cw} - F_{cd} \quad (4)$$

where C_T is the amount of carbon in the ocean–atmosphere system.

The major sources of alkalinity are the weathering of continental carbonates and silicates (F_{cw} and F_{sw}). F^D_{sw} is the alkalinity flux from Deccan basalt weathering. As for carbon, the carbonate deposition on the seafloor (F_{cd}) is the major sink of alkalinity. The long-term budget can be written as:

$$\frac{dA_T}{dt} = 2(F^D_{sw} + F^R_{sw} + F_{cw} - F_{cd}) \quad (5)$$

where A_T is the amount of alkalinity in the ocean.

The source of ocean strontium is the weathering of silicate and carbonate rocks and its major sink is the carbonate precipitation. The strontium budget is hence determined by:

$$\frac{dSr_T}{dt} = k^D_{sw}F^D_{sw} + k^R_{sw}F^R_{sw} + k_{cw}F_{cw} - k_{cd}F_{cd} \quad (6)$$

where k^D_{sw}, k^R_{sw}, k_{cw} and k_{cd} are proportionality factors used to transform carbon or alkalinity fluxes into strontium fluxes [44]. They are considered constant and are obtained from the ratios between strontium and carbon fluxes of today (Table 3).

The evolution of the $^{87}Sr/^{86}Sr$ isotopic ratio of ocean water over geologic time can be written as:

$$Sr_T\frac{dr_{oc}}{dt} = (r^D_{sw} - r_{oc})k^D_{sw}F^D_{sw} + (r^R_{sw} - r_{oc})k^R_{sw}F^R_{sw} +$$

$$(r_{cw} - r_{oc})k_{cw}F_{cw} + (r_{sfw} - r_{oc})k_{sfw}F^R_{vol} \quad (7)$$

$k_{sfw}F^{R}_{vol}$ is the exchange flux of Sr during seafloor basalt alteration which is considered to be proportional to the non-Deccan volcanic CO_2 flux F^{R}_{vol}. r_{oc} is the strontium isotopic ratio of the ocean [45] and r^{D}_{sw}, r^{R}_{sw}, r_{cw} and r_{sfw} are the mean strontium isotopic ratios originating from Deccan basalts, silicate weathering, carbonate weathering and seafloor basalt alteration [46]. Note that carbonate deposition is not taken into account in the isotopic budget (Eq. 7) because it is assumed that no fractionation occurs during precipitation. The diagenetic flux is small enough that it can be ignored with no significant lack of accuracy in Eqs. 6 and 7. The values of some present-day model parameters are given in Table 3 with relevant references. The riverine $^{87}Sr/^{86}Sr$ ratio coming from Deccan Traps weathering (r^{D}_{sw}) used in the model is the present-day ratio. Because of the low ratio Rb/Sr of Deccan basalts [34,36], the chronological correction is insignificant and we can suppose that the riverine $^{87}Sr/^{86}Sr$ ratio coming from Deccan Traps weathering has not significantly changed over the last 65 Myr. The oceanic $^{87}Sr/^{86}Sr$ ratio before Deccan Traps emplacement was determined from the actual marine Sr isotope record 65 Myr ago [45] and is equal to 0.7078. From this value and the present-day fluxes of strontium, we have calculated the pre-Deccan $^{87}Sr/^{86}Sr$ ratio of global riverine flux (0.7103) and riverine flux coming from silicate weathering excluding Deccan ($r^{R}_{sw} = 0.7115$).

Over geologic time, weathering fluxes are affected by various factors such as continental surface (A), global average runoff per unit area (R_f), surface temperature (T) and atmospheric CO_2 concentration (pCO_2). In this model, we use the BLAG relations [2] that link R_f to T and pCO_2 to T:

$$\frac{R_f}{R_{f0}} = 1 + 0.038 \times (T - T_0) \quad (8)$$

$$T = T_0 + 2.88 \times \ln\left(\frac{pCO_2}{pCO_{2,0}}\right) \quad (9)$$

where the 0 subscript refers to present-day values (280 ppmv and 288 K respectively for pre-industrial pCO_2 and T).

In the case of silicate rocks, weathering fluxes are proportional to runoff, temperature and continental area. The global flux (F_{sw}) is the sum of the Deccan Traps contribution and that of the rest of the world. Each contribution is described

Table 3
Main parameters of the geochemical model

Parameter	Value	Reference
CO_2 consumption flux by carbonate weathering	12.3×10^{12} mol/yr	[3]
CO_2 consumption by silicate weathering	11.7×10^{12} mol/yr	[3]
CO_2 release from Deccan Traps pulses	1.6×10^{18} mol	[35]
CO_2 consumption by weathering of Deccan basalts	0.63×10^{12} mol/yr	This study
Riverine flux of Sr	28.4×10^{9} mol/yr	Calibrated from CO_2 flux and k values
k_{cw}	1/1250	[44]
k^{R}_{sw}	1/305	[44]
k^{D}_{sw}	1/840	This study
k_{sfw}	1/140	[44]
Oceanic $^{87}Sr/^{86}Sr$ ratio before Deccan Traps emplacement, r_{oc}	0.7078	[45]
Global riverine $^{87}Sr/^{86}Sr$ ratio before Deccan Traps emplacement	0.7103	Calibrated to obtain an oceanic $^{87}Sr/^{86}Sr$ of 0.7078
Riverine $^{87}Sr/^{86}Sr$ ratio coming from carbonate weathering, r_{cw}	0.7080	[46]
Riverine $^{87}Sr/^{86}Sr$ ratio coming from Deccan Traps weathering, r^{D}_{sw}	0.7097	This study
Riverine $^{87}Sr/^{86}Sr$ ratio coming from silicate weathering, r^{R}_{sw} (excluding Deccan)	0.7115	Calibrated to obtain a riverine $^{87}Sr/^{86}Sr$ of 0.7103
$^{87}Sr/^{86}Sr$ ratio coming from seafloor basalt weathering, r_{sfw}	0.7030	[45]

by the following equation:

$$\frac{F^{i}_{sw}}{F^{i}_{sw0}} = \frac{A}{A_0} \times \frac{R_f}{R_{f0}} \times \exp\left[-\frac{Ea_i}{R}\left(\frac{1}{T}-\frac{1}{T_0}\right)\right] \quad (10)$$

with i = D or R.

A/A_0 is the area (Deccan Traps or rest of the world) normalised to today's value. R is the gas constant and Ea is the activation energy of the mineral dissolution reaction. An apparent energy of 42.5 kJ/mol and 40 kJ/mol is used for Deccan basalt dissolution (determined in Section 5) and dissolution of silicates from the rest of the world (unpublished data of Oliva), respectively. Before the emplacement of Deccan basalts, we suppose that this area was constituted by silicates as in the rest of the world (with $Ea = 40$ kJ/mol) and that the system was at steady state. To calculate carbonate weathering, it is assumed that stream water draining carbonate lithologies reaches equilibrium with calcite and an effective pCO_2 value (pCO_2^{eff}), which is a harmonic mean between soil and atmospheric pCO_2. Soil pCO_2 is calculated according to Volk's [47] study with a present value 100 times higher than the atmospheric value.

The ocean sub-model allows us to estimate atmospheric pCO_2 and F_{cd} values for all C_T and A_T combinations determined at each time step of the numeric resolution (Eqs. 4 and 5). This sub-model contains three surface pools: the atmosphere, the surface ocean and the deep ocean, and distributes instantaneously C_T and A_T between these three boxes. As these boxes are assumed to be in equilibrium with each other, the model cannot be used to analyse the evolution of the system at time scales shorter than 1000 years (oceanic circulation). Carbonate speciation in each oceanic reservoir is taken into account to calculate atmospheric pCO_2 in equilibrium with the surface ocean and to determine the lysocline depth for aragonite and calcite from the calculated CO_3^{2-} concentrations. Carbon is transferred between the surface and the deep ocean reservoir through advective exchange (ocean circulation) and sedimentation of biological particles. The biological new production is constant in all of the simulations. The flux of carbonate deposition F_{cd} is composed of the aragonite and carbonate tests deposited above their respective lysocline (i.e. these fluxes are proportional to the fraction of the seafloor area located above the aragonite or calcite lysocline), as well as of coral reef formation on the equatorial shelf.

7.2. Results

7.2.1. Reference simulation

The reference run combines all the effects presented previously. The calculated evolutions of surface temperature (°C), atmospheric pCO_2 (ppmv), carbonate deposition on seafloor (10^{13} mol/yr), surface ocean pH and $^{87}Sr/^{86}Sr$ ratio of seawater during the emplacement of the traps are shown in Figs. 4–6.

The variation of atmospheric pCO_2 is relatively important. In fact, pCO_2 increases by 1050 ppmv from its pre-Deccan steady-state value. It then progressively decreases to reach a new (post-Dec-

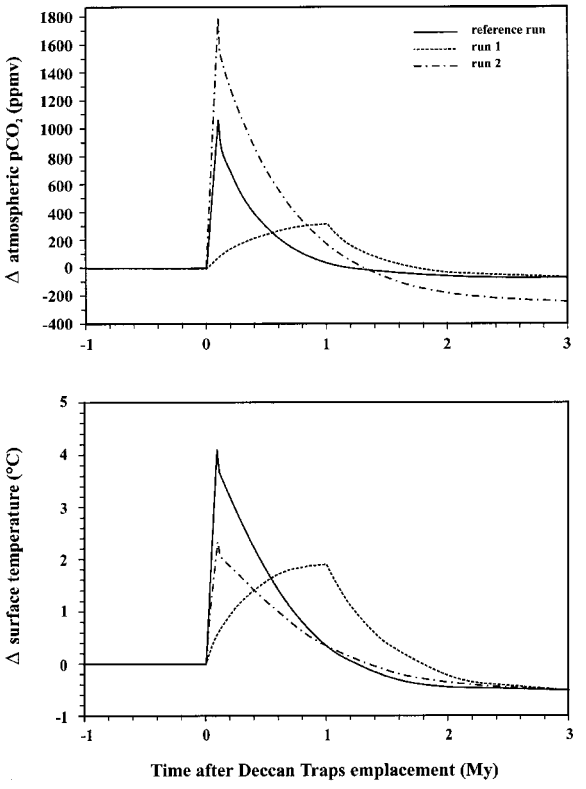

Fig. 4. The evolution of atmospheric CO_2 partial pressure (ppmv) and surface temperature (°C) calculated from the different model runs described in the text.

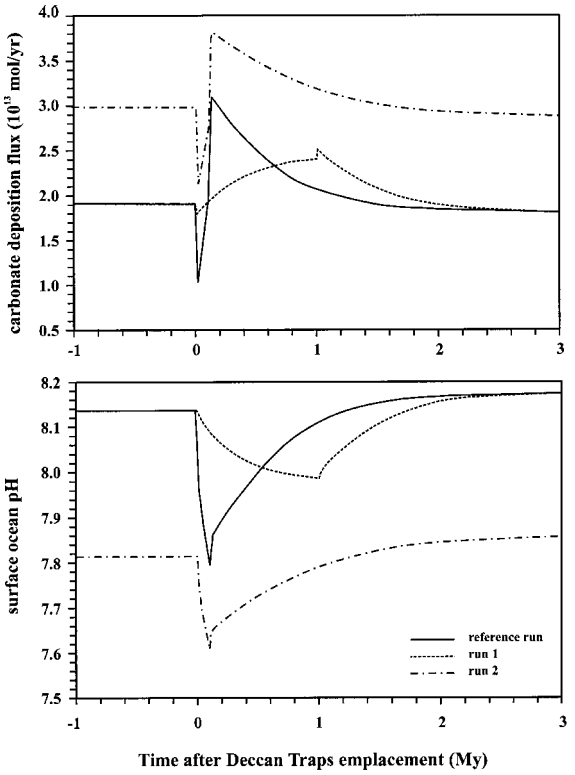

Fig. 5. The evolution of the carbonate deposition flux in the ocean (10^{13} mol/yr) and surface ocean pH calculated from the different model runs.

can) steady state after a few million years. Note that only 1.2 Myr is necessary to return to the pre-Deccan value. After 1.2 Myr, pCO_2 continues to decrease and the new steady-state pCO_2 is lower than the pre-Deccan one by 57 ppmv, as a result of the very efficient weathering of the Deccan basalts. Thus, the emplacement of Deccan Traps appears to be responsible for a 20% reduction of atmospheric pCO_2 (with respect to pre-industrial pCO_2). This decrease is accompanied by a global cooling of 0.55°C.

The variation of carbonate deposition is greater than in the case of atmospheric pCO_2 and surface temperature (Fig. 5). Indeed, this flux first decreases by 0.87×10^{13} mol/yr (−45%) from its pre-Deccan value in only 20 000 years, as a result of a rapid rise of the lysocline. This is followed by a rapid rise in carbonate deposition of 2.05×10^{13} mol/yr, resulting in a strong increase of continental erosion. Finally, it progressively decreases to reach steady state after 1.4 Myr. On the other hand, it can be seen that the surface ocean pH decreases rapidly from 8.13 to 7.80 in 0.1 Myr. Note that this decrease is more rapid during the first 20 000 years. After 0.1 Myr, the time corresponding to the end of Deccan emplacement, the pH progressively increases to reach a steady-state value of 8.17. These two parameters demonstrate the immediate response of ocean and continents to regulate the strong input of CO_2 in the atmosphere.

After the beginning of Deccan eruption, the $^{87}Sr/^{86}Sr$ ratio of seawater increased from its pre-Deccan value of 0.70782 to 0.70789, before coming down to 0.70777 (Fig. 6). This spike is characterised by a duration of some 4 Myr and a peak amplitude of about 7×10^{-5}. The transient peak in the Sr signal is related to the strong increase of continental weathering during and after the eruption. As pCO_2 decreases, continental weathering rates are reduced leading to a decrease in oceanic $^{87}Sr/^{86}Sr$ ratio. Furthermore, as r_{sw}^{D} is lower than r_{sw}^{R}, the weathering of Deccan Traps tends to reduce the global isotopic ratio of strontium originating from silicate weathering.

Note that the Deccan Traps cover 0.5×10^{6} km^2, but their original area was three or four times larger. In this respect, the impact of these traps is underestimated.

7.2.2. Test simulations

In order to explore the contribution of various parameters, several sensitivity tests were performed such as the duration of the emplacement, the pre-Deccan atmospheric pCO_2, the contribution of the erosion of continental carbonates and the dependence of silicate weathering on atmospheric pCO_2. As most of the results of the simulations are relatively close to that of the reference one, only the two more significant ones are presented in this study (Figs. 4–6).

The first important sensitivity test (run 1) was performed to analyse the impact of the duration of emplacement of Deccan Traps. In this test, the 1.6×10^{18} mol of CO_2 were released to the atmosphere in 1 Myr instead of 10^5 years in the reference run. The characteristic peak of pCO_2 during Deccan Traps emplacement is strongly reduced in

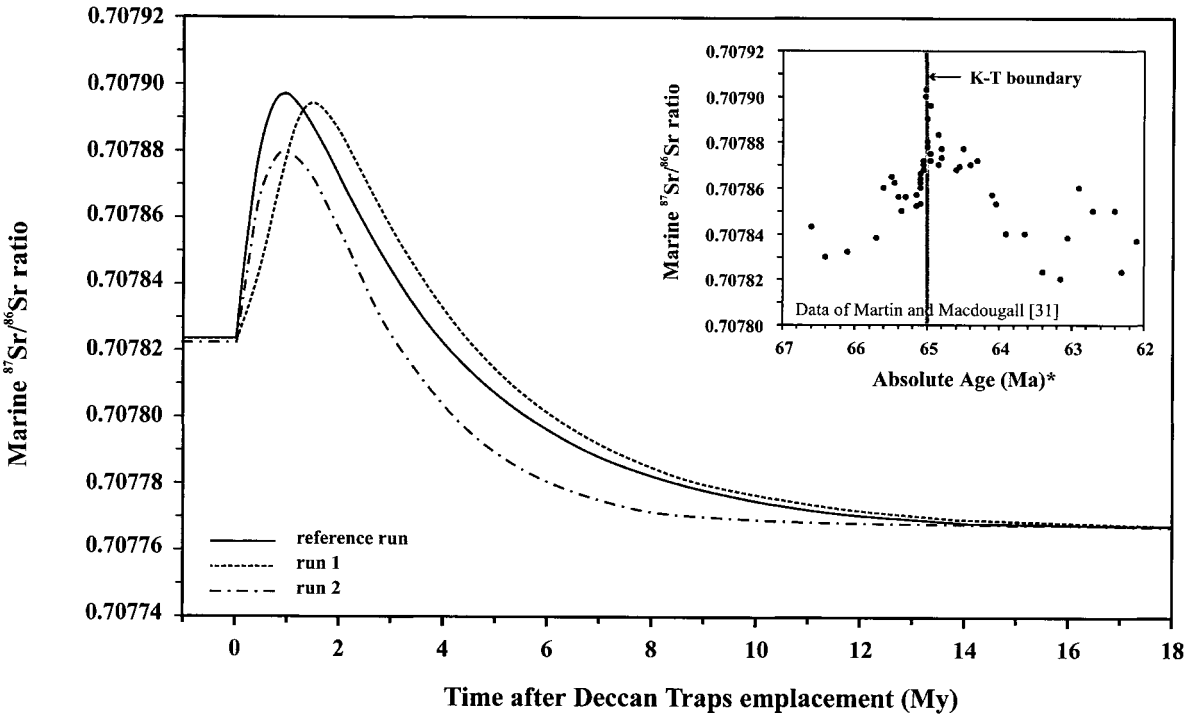

Fig. 6. The evolution of the seawater $^{87}Sr/^{86}Sr$ ratio calculated from the different model runs. By comparison, the data points represent the marine Sr isotope record taken from Martin and Macdougall [31] around the KT boundary. *: absolute age based on Martin and Macdougall was recalibrated from 65 Ma (KT boundary).

this simulation, pCO_2 increasing by only 317 ppmv. This smaller variation reduces the impact on global temperature. The return to the post-Deccan steady-state value is longer (1.7 Myr instead of 1.2 Myr) and the spike of carbonate deposition is weak. Indeed, after a small decrease of 5%, carbon deposition flux progressively increases by 0.6×10^{13} mol/yr, before returning to steady state, about 2 Myr after the beginning of Deccan eruption. Similarly, in comparison with the reference simulation we do not observe any important variation of surface ocean pH. A delay is also observed in the Sr signal, where the peak appears 1.4 Myr after the beginning of the eruption. This simulation illustrates the role of duration of Deccan Traps emplacement at short time scales.

In the second sensitivity test (run 2), the pre-Deccan atmospheric pCO_2 is assumed higher than in the reference one. To get high CO_2 levels, the CO_2 release from pre-Deccan volcanism (F^{R}_{vol}) was increased by a factor of 1.5. This larger volcanic flux resulted in a pre-Deccan atmospheric CO_2 of 1435 ppmv and a global surface temperature of 292.7 K. Under such high levels of CO_2, the evolution of pCO_2 following Deccan Traps emplacement is perceptibly different. Atmospheric pCO_2 increases by 1792 ppmv after emplacement and returns to a new steady-state pCO_2 lower than that in pre-Deccan times by 260 ppmv. On the other hand, the increase of pre-Deccan pCO_2 has a smaller effect on the variation of global temperature. Indeed, the warming related to the CO_2 degassing phase is smaller than the reference one (2.3°C instead of 4.1°C) and the global cooling is unchanged. We note that, as a result of higher volcanic pCO_2 fluxes, the carbonate deposition flux is higher than the reference one. The pH is relatively low (as expected under high pCO_2) and its variation is smaller. The increase of pre-Deccan pCO_2 also has an effect on the

marine Sr record since the spike is characterised by an amplitude (peak at 0.70788) and a duration (3 Myr) smaller than the reference one. This simulation illustrates that, even if the increase of pre-Deccan pCO_2 has a global effect on silicate weathering and the Sr cycle, the impact of Deccan Traps emplacement is reduced.

7.2.3. *Comparison between results of model and marine sediment records*

We have shown that Deccan Traps emplacement had multiple effects on the global environment. We propose that this event caused a sharp decrease in sedimentation (−45% in only 20 kyr), induced by a strong change in lysocline depth. This disturbance and decrease of carbonate deposition has also been observed at the KT boundary by several authors including Smit and Romein [48] and Kaiho et al. [49] who inferred a 13 kyr interval of productivity shutdown. The simulations involve a rapid increase of seawater $^{87}Sr/^{86}Sr$ ratio of 8×10^{-5} with a duration of 4 Myr; therefore the emplacement and weathering of these continental flood basalts may explain the very abrupt KT boundary spike in $^{87}Sr/^{87}Sr$ [29–31].

In order to validate the model, we compare our simulations of oceanic $^{87}Sr/^{86}Sr$ evolution with the actual marine Sr isotope record around the KT boundary of Martin and Macdougall [31] in Fig. 6. To reduce variability due to chronological uncertainty, sediment mixing, analytical uncertainty and diagenesis, the authors have smoothed and replotted the data. In this study the KT boundary is assimilated to the spike in $^{87}Sr/^{86}Sr$ at 66.4 Ma. We recalibrated the age of this boundary at 65 Ma, its well known age. The data of Martin and Macdougall show a spike with a peak value of about 0.7079, a maximum amplitude of order 7×10^{-5} and a maximum duration of 3 Myr that is relatively similar to the evolution proposed in our model. This study allows us to suggest an origin for the Sr isotope anomaly at the KT boundary.

The results of the model show that a number of geochemical characteristics of the KT boundary can be explained by Deccan Traps emplacement.

8. Conclusion

This study presents a coupled geochemical investigation of major and trace elements of the main rivers draining the Deccan Traps province as well as a simple model making it possible to quantify the impact of Deccan Traps emplacement.

- The chemical composition of the dissolved load in the main rivers draining Deccan Traps basalts allows us to calculate chemical weathering rates (21–63 t/km^2/yr) and associated atmospheric CO_2 consumption rates (0.58–2.54 10^6 mol C/km^2/yr). The results obtained in this study confirm that denudation rates of basaltic rocks are much higher than those for other silicate rocks. Furthermore, it is suggested that runoff and temperature are the most important parameters which control the chemical weathering and CO_2 consumption rates, which can be rather accurately described by a simple exponential law:

$$f = R_f \times C_0 \exp\left[\frac{-Ea}{R}\left(\frac{1}{T}-\frac{1}{298}\right)\right]$$

  where f is the specific CO_2 consumption rate (mol/km^2/yr), R_f is runoff (mm/yr), $C_0 = 1764$ μmol/l, Ea represents an apparent activation energy for basalt weathering (42.3 kJ/mol), R is the gas constant and T is the absolute temperature (°K).
- Our model allows one to quantify the multiple effects of Deccan Traps emplacement on the global environment. This emplacement is responsible for a 20% reduction of atmospheric pCO_2, accompanied by a global cooling of 0.55°C, and has therefore produced a net CO_2 sink on geologic time scales. A peak in the $^{87}Sr/^{86}Sr$ isotopic ratio in the oceans following Deccan Traps emplacement is also predicted by the model and indeed allows one to understand the origin of the Sr isotope anomaly at the KT boundary.
- Overall, this study emphasises the major impact of basalt weathering on geochemical cycles such as the carbon cycle. It shows that the emplace-

ment and the weathering of large basaltic provinces cannot be neglected when attempting to better understand the geochemical and climatic evolution of the Earth.

Acknowledgements

This work was supported by the French programme PROSE (Programme Recherche Sol Erosion) funded by INSU. We also thank the Foreign Office and the French Ministry of Education, Research and Technology for funding and providing post-doctoral positions for G.J.C. and S.B. L.M.F. was supported by the FNRS (Belgian National Foundation for Scientific Research) and obtained from a visiting research position from CNRS. We would like to thank V. Subramanian and the technicians of the School of Environmental Sciences, New Delhi, as well as N. Vigier and T. Allard for assistance in obtaining river samples. We are also grateful to P. Brunet, J. Escalier, P. Oliva, B. Reynier, M. Valladon of the Toulouse laboratory and to F. Capmas, C. Gorge and M. Pierre of IPGP for their support in the different analyses. L. Turpin, N. Vigier, J. Viers and P. Oliva are thanked for their helpful comments. We thank V. Courtillot and C. France-Lanord for their very constructive reviews of this manuscript. *[AC]*

References

[1] R.M. Garrels, F. Mackenzie, Evolution of Sedimentary Rocks, Norton, New York, 1971.

[2] R.A. Berner, A.C. Lasaga, R.M. Garrels, The carbonate-silicate geochemical cycle and its effect on atmospheric carbon dioxide over the past 100 millions years, Am. J. Sci. 284 (1983) 641–683.

[3] J. Gaillardet, B. Dupré, P. Louvat, C.J. Allègre, Global silicate weathering and CO_2 consumption rates deduced from the chemistry of the large rivers, Chem. Geol. 159 (1999) 3–30.

[4] C. France-Lanord, L.A. Derry, Organic carbon burial forcing of the carbon cycle from Himalaya erosion, Nature 390 (1997) 65–67.

[5] J.M. Hayes, H. Strauss, A.J. Kaufman, The abundance of ^{13}C in marine organic matter and isotopic fractionation in the global biogeochemical cycle of carbon during the past 800 Ma, Chem. Geol. 161 (1999) 103–125.

[6] M.E. Raymo, The Himalayas, organic carbon burial, and climate in the Miocene, Paleoceanography 9 (1994) 399–404.

[7] A.J. Spivack, H. Staudigel, Low-temperature alteration of the upper oceanic crust and the alkalinity budget of seawater, Chem. Geol. 115 (1994) 239–247.

[8] L.M. François, J.C.G. Walker, Modelling the Phanerozoic carbon cycle and climate: constraints from the $^{87}Sr/^{86}Sr$ isotopic ratio of seawater, Am. J. Sci. 292 (1992) 81–135.

[9] J.C.G. Walker, P.B. Hays, J.F. Kasting, A negative feedback mechanism for the long-term stabilization of Earth's surface temperature, J. Geophys. Res. 86 (1981) 9776–9782.

[10] O. Brevart, C.J. Allègre, Strontium isotopic ratios in limestone through geological time as a memory of geodynamic regimes, Sci. Geol. Bull. 19 (1977) 1253–1257.

[11] R.F. Stallard, J.M. Edmond, Geochemistry of the Amazon 2. The influence of geology and weathering environment on the dissolved load, J. Geophys. Res. 88 (C14) (1983) 9671–9688.

[12] P. Négrel, C.J. Allègre, B. Dupré, E. Lewin, Erosion sources determined by inversion of major and trace element ratios and strontium isotopic ratios in river water: The Congo Basin case, Earth Planet. Sci. Lett. 120 (1993) 59–76.

[13] J.M. Edmond, M.R. Palmer, C.I. Measures, B. Grant, R.F. Stallard, The fluvial geochemistry and denudation rate of the Guyana Shield in Venezuela, Colombia, and Brazil, Geochim. Cosmochim. Acta 59 (1995) 3301–3325.

[14] B. Dupré, J. Gaillardet, D. Rousseau, C.J. Allègre, Major and trace elements of river borne material: The Congo Basin, Geochim. Cosmochim. Acta 60 (1996) 1301–1321.

[15] J. Gaillardet, B. Dupré, C.J. Allègre, A global geochemical mass budget applied to the Congo Basin rivers: erosion rates and continental crust composition, Geochim. Cosmochim. Acta 59 (1995) 3469–3485.

[16] J. Gaillardet, B. Dupré, C.J. Allègre, P. Négrel, Chemical and physical denudation in the Amazone River Basin, Chem. Geol. 142 (1997) 141–173.

[17] A. Galy, C. France-Lanord, Weathering processes in the Ganges-Brahmaputra basin and the riverine alkalinity budget, Chem. Geol. 159 (1999) 31–60.

[18] J.L. Probst, J. Mortatti, Y. Tardy, Carbon river fluxes and weathering CO_2 consumption in the Congo and Amazon river basins, Appl. Geochem. 9 (1994) 1–13.

[19] M. Meybeck, Composition chimique des ruisseaux non pollués de France, in: Sciences Geologiques 39, Strasbourg, 1986, pp. 3–77.

[20] S.R. Gislason, S. Arnorsson, H. Armannsson, Chemical weathering of basalt as deduced from the composition of precipitation, rivers and rocks in SW Iceland, Am. J. Sci. 296 (1996) 837–907.

[21] P. Louvat, C.J. Allègre, Present denudation rates at Réunion island determined by river geochemistry: basalt

weathering and mass budget between chemical and mechanical erosions, Geochim. Cosmochim. Acta 61 (1997) 3645–3669.
[22] G.J.S. Bluth, L.R. Kump, Lithologic and climatic control of river chemistry, Geochim. Cosmochim. Acta 58 (1994) 2341–2359.
[23] A.F. White, A.E. Blum, Effects of climate on chemical weathering in watersheds, Geochim. Cosmochim. Acta 59 (1995) 1729–1747.
[24] P. Amiotte-Suchet, J.L. Probst, A global model for present-day atmospheric/soil CO_2 consumption by chemical erosion of continental rocks (GEM-CO2), Tellus 47B (1995) 273–280.
[25] P. Louvat, Etude géochimique de l'érosion fluviale d'iles volcaniques à l'aide des bilans d'éléments majeurs et traces, Ph.D. Thesis, Université Paris 7, 1997.
[26] A.S. Taylor, A.C. Lasaga, The role of basalt weathering in the Sr isotope budget of the oceans, Chem. Geol. 161 (1999) 199–214.
[27] V. Courtillot, J. Besse, D. Vandamme, R. Montigny, J.J. Jaeger, H. Cappetta, Deccan flood basalt at the Cretaceous/Tertiary boundary?, Earth Planet. Sci. Lett. 80 (1986) 361–374.
[28] C.J. Allègre, J.L. Birck, F. Capmas, V. Courtillot, Age of the Deccan Traps using ^{187}Re–^{187}Os systematics, Earth Planet. Sci. Lett. 170 (1999) 197–204.
[29] D.J. DePaolo, B.L. Ingram, High-resolution stratigraphy with strontium isotopes, Science 227 (1985) 938–941.
[30] J. Hess, M.L. Bender, J.G. Schilling, Evolution of the ratio of strontium-87 to strontium-86 in seawater from Cretaceous to present, Science 231 (1986) 979–984.
[31] E.E. Martin, J.D. Macdougall, Seawater Sr isotopes at the Cretaceous/Tertiary boundary, Earth Planet. Sci. Lett. 104 (1991) 166–180.
[32] V. Courtillot, C. Jaupart, I. Manighetti, P. Tapponnier, J. Besse, On causal links between flood basalts and continental breakup, Earth Planet. Sci. Lett. 166 (1999) 177–195.
[33] J. Besse, V. Courtillot, Paleogeographic maps of the continents bordering the Indian Ocean since the Early Jurassic, J. Geophys. Res. 93 (1988) 11791–11808.
[34] P. Ligtfoot, C.J. Hawkesworth, Origin of Deccan Trap lavas: evidence from combined trace element and Sr-, Nd- and Pb-isotope studies, Earth Planet. Sci. Lett. 91 (1988) 89–104.
[35] M. Javoy, G. Michard, Am. Geophys. Union EOS Trans. 70 (1989) 1421.
[36] K.G. Cox, C.J. Hawkesworth, Geochemical stratigraphy of the Deccan Traps at Mahabaleshwar, Western Ghats, India, with implications for open system magnetic processes, J. Petrol. 26 (1985) 355–377.
[37] C.W. Devey, P.C. Lightfoot, Volcanological and tectonic control of stratigraphy and structure in the western Deccan Traps, Bull. Volcanol. 48 (1986) 195–207.
[38] J.J. Mahoney, Deccan traps, in: J.D. Macdougall (Ed.), Continental Flood Basalts, Petrology and Structural Geology, Kluwer Academic, Dordrecht, 1989, pp. 151–194.
[39] M. Widdowson, K.G. Cox, Uplift and erosional history of the Deccan Traps, India: Evidence from laterites and drainage patterns of the Western Ghats and Konkan Coast, Earth Planet. Sci. Lett. 137 (1996) 57–69.
[40] D.V. Borole, S. Krishnaswami, B.L.K. Somayajulu, Uranium isotopes in rivers, estuaries and adjacent coastal sediments of western India: their weathering, transport and oceanic budget, Geochim. Cosmochim. Acta 46 (1982) 125–137.
[41] V.M. Dekov, V. Subramanian, R. Van Grieken, Chemical composition of suspended matter and sediments from the India Sub-continent: a fifteen-year research survey, in: Recent Trends in Environmental Biogeochemistry, ENVIS Centre, School of Environmental Sciences, Jawaharlal Nehru University, New Delhi, 1998, pp. 81–92.
[42] M.F. Benedetti, O. Menard, Y. Noack, A. Carvalho, D. Nahon, Water rock interactions in tropical catchments: field rates of weathering and biomass impact, Chem. Geol. 118 (1994) 203–220.
[43] L.M. François, J.C.G. Walker, B.N. Opdyke, The history of global weathering and the chemical evolution of the ocean-atmosphere system, in: E. Takahashi, R. Jeanloz, D. Dubie (Eds.), Evolution of the Earth and Planets, Vol. 14, International Union of Geodesy and Geophysics and the American Geophysical Union, Washington, DC, 1993, pp. 143–159.
[44] K. Semhi, Erosion et transferts de matières sur le bassin de la Garonne. Influence de la sécheresse, Ph.D. Thesis, Université Strasbourg I, 1996.
[45] F.M. Richter, D.B. Rowley, D.J. DePaolo, Sr isotope evolution of seawater: the rôle of tectonics, Earth Planet. Sci. Lett. 109 (1992) 11–23.
[46] M.R. Palmer, J.M. Edmond, The strontium isotope budget of the modern ocean, Earth Planet. Sci. Lett. 92 (1989) 11–26.
[47] T. Volk, Feedbacks between weathering and atmospheric CO_2 over the last 100 million years, Am. J. Sci. 287 (1987) 763–779.
[48] J. Smit, A.J.T. Romein, A sequence of events across the Cretaceous–Tertiary boundary, Earth Planet. Sci. Lett. 74 (1985) 155–170.
[49] K. Kaiho, Y. Kajiwara, K. Tazaki, M. Ueshima, N. Takeda, H. Kawahata, T. Arinobu, R. Ishiwatari, A. Hirai, M.A. Lamolda, Oceanic primary productivity and dissolved oxygen levels at the Cretaceous/Tertiary boundary: Their decrease, subsequent warming, and recovery, Paleoceanography 14 (1999) 511–524.